Lecture 8

Bounds for Rotating Fluids

P. Constantin

Notes by U. Riemenschneider and S. Plasting

1 Introduction

Bounding problems in fluid turbulence have classically been concerned with finding bounds on one point quantities such as the time and space averaged dissipation rate $\mathcal{F}(Re) = \nu \left\langle \|\nabla \mathbf{u}\|^2 \right\rangle$. Another class of problem is to find bounds on two point quantities which depend both on the system control parameter and on a space- or time-like parameter. An example of such a quantity is the energy spectrum $E(k; Re) = \frac{1}{t} \int_0^t |\hat{\mathbf{u}}(k)|^2 \mathrm{d}t$, where k is the magnitude of the wave number, which is the density of the contributions to the kinetic energy on the wave-number magnitude axis. The total kinetic energy is $\frac{1}{2t} \int_0^t \|\mathbf{u}\|^2 \mathrm{d}t = \int_0^\infty E(k) \mathrm{d}k$.

This lecture deals with deriving rigorous upper bounds on transport quantities and energy spectra for rotating fluid systems. We present results for bounds on one and two point quantities which are derived by following the Constantin-Doering-Hopf bounding approach.

2 Bounds for Rayleigh-Bénard Convection

The effect of rotation on convective heat transport is an important issue in astrophysical and geophysical applications. Here we shall consider the heat transport through a fluid layer confined between two parallel plates heated from below with fixed temperature on both top and bottom plates, which is rotating with a constant rate around an axis of rotation perpendicular to the plates. No-slip boundary conditions will be assumed throughout. The non-dimensional equations for Boussinesq convection with rotation are

$$\frac{1}{Pr} \left(\frac{\partial \mathbf{u}}{\partial t} + \mathbf{u} \cdot \boldsymbol{\nabla} \mathbf{u} \right) + E^{-1} \hat{\mathbf{k}} \times \mathbf{u} + \boldsymbol{\nabla} p = \Delta \mathbf{u} + Ra \hat{\mathbf{k}} T \tag{1}$$

$$\boldsymbol{\nabla} \cdot \mathbf{u}$$

$$\frac{\partial T}{\partial t} + \mathbf{u} \cdot \boldsymbol{\nabla} T = \Delta T$$

where the Prandtl number is defined as $Pr = \nu/\kappa$, the Ekman number is inversely proportional to the rotation rate, and the Rayleigh number is the standard non-dimensionalised temperature difference across the fluid layer.

In the limit of infinite Prandtl number one can neglect the inertial terms of the left hand side of Equation (1). In the remaining system of equations T is the active scalar and the velocity vector $\mathbf{u}$ is linearly dependent on T. In the bounding analysis of this problem the full momentum equation can be utilised as a pointwise constraint due to its

linearity. Following the derivation in [1] we are able to show that the following equations in the vertical component of velocity $w = \hat{\mathbf{k}} \cdot \mathbf{u}$ and the vertical component of vorticity $\xi = \hat{\mathbf{k}} \cdot (\boldsymbol{\nabla} \times \mathbf{u})$ fully determine the dynamics of the convective state

$$\Delta^2 w - E^{-1} \frac{\partial \xi}{\partial z} = -Ra \Delta_{_H} T \tag{2}$$

$$-\Delta \xi - E^{-1} \frac{\partial w}{\partial z} = 0 \tag{3}$$

subject to the boundary conditions

$$w = \frac{\partial w}{\partial z} = 0 = \xi \quad \text{ at } z = 0,\, 1.$$

Multiplying Equation (2) by w, Equation (3) by ξ, adding and integrating we deuce that the following E-independent bound holds pointwise in time

$$\boxed{\|\Delta w\|^2 + 2\|\Delta \xi\|^2 \leq Ra^2} \tag{4}$$

where we use a normalised L^2 norm

$$\|f\|^2 = \frac{1}{L^2} \int_0^1 \int_0^L \int_0^L |f(x,y,z)|^2 dx\, dy\, dz.$$

Equation (3) can be rearranged to

$$\boxed{\frac{\partial w}{\partial z} = -E \Delta \xi} \tag{5}$$

The previous two expressions together imply that for strong rotation rates ($E \to 0$) horizontal variations in w are restricted and a stratification is set up such that a purely conductive state is realised.

The total non-dimensional heat transport is quantified by the Nusselt number which is defined as the long-time average of the vertical heat flux

$$N = 1 + \left\langle \int_0^1 b(z,t) dz \right\rangle$$

where

$$b(z,t) := \frac{1}{L^2} \int_0^L \int_O^L w(x,y,z,t)\, T(x,y,z,t) dx\, dy.$$

and $\langle \cdot \rangle$ is used to denote the long-time average

$$\langle f \rangle = \limsup_{t = \to \infty} \frac{1}{t} \int_0^t f(s) ds.$$

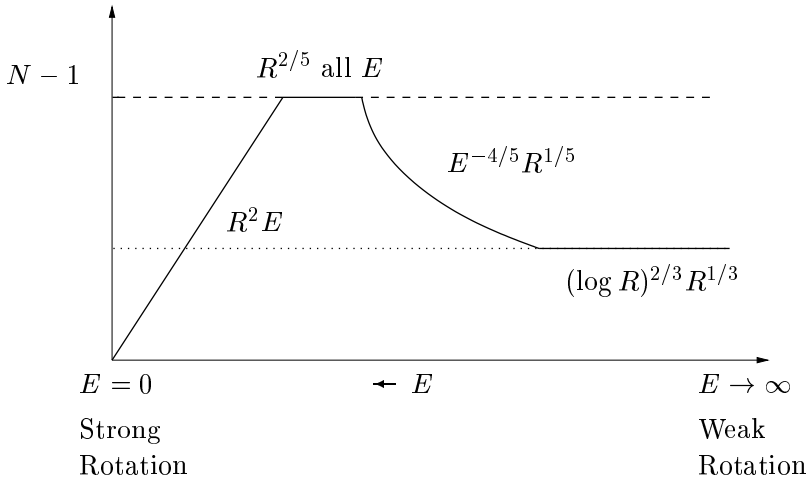

Figure 1: A plethora of upper bounds on the heat transport, N, in Rayleigh-Bénard convection for infinite Prandtl number.

Figure (1) shows the results of several upper bounding studies for the infinite Prandtl number problem. Upper bounds on $N-1$ are plotted against the Ekman number. The top most upper bound is a uniform bound in E [2]. Intersecting this bound are two other upper bounds. The bound to the left has the proper qualitative dependence on rotation in that convection is suppressed in the limit of strong rotation ($E \to 0$) which is suggested by the relations in (4) and (5) [3]. In the absence of rotation ($E = \infty$) a logarithmic bound has been obtained [4], which is illustrated by the dotted line in the figure. Allowing for finite E they find in [1] that there is a region in which the optimal bound is lowered from $R^{2/5}$ and connects to the logarithmic bound at some higher Ekman number.

3 Bounds on the Energy Spectrum

We now turn our attention to a problem for which an upper bound on the scaling of the energy spectrum in rotating turbulence has been caculated.

3.1 Motivating Experiment of H. L. Swinney

The motivation is a recent experiment by Baroud, Plapp, She and Swinney [5] for which Kolmogorov's theory for two-dimensional turbulence does not justify the scaling of the energy spectrum in the inverse cascade region. In the Experiment quasi-two-dimensional flow is studied in a rapidly rotating cylindrical annulus. The resulting velocity measurements yield a self-similar probability distribution function for longitudinal velocity differences, which are strongly non-Gaussian. The resulting energy spectrum is described by $E(k) \sim k^{-2}$ rather than the expected $E(k) \sim k^{-5/3}$ from Kolmogorov's theory. We shall outline a brief background to Kolmogorov's statistical study of turbulence, followed by a description of

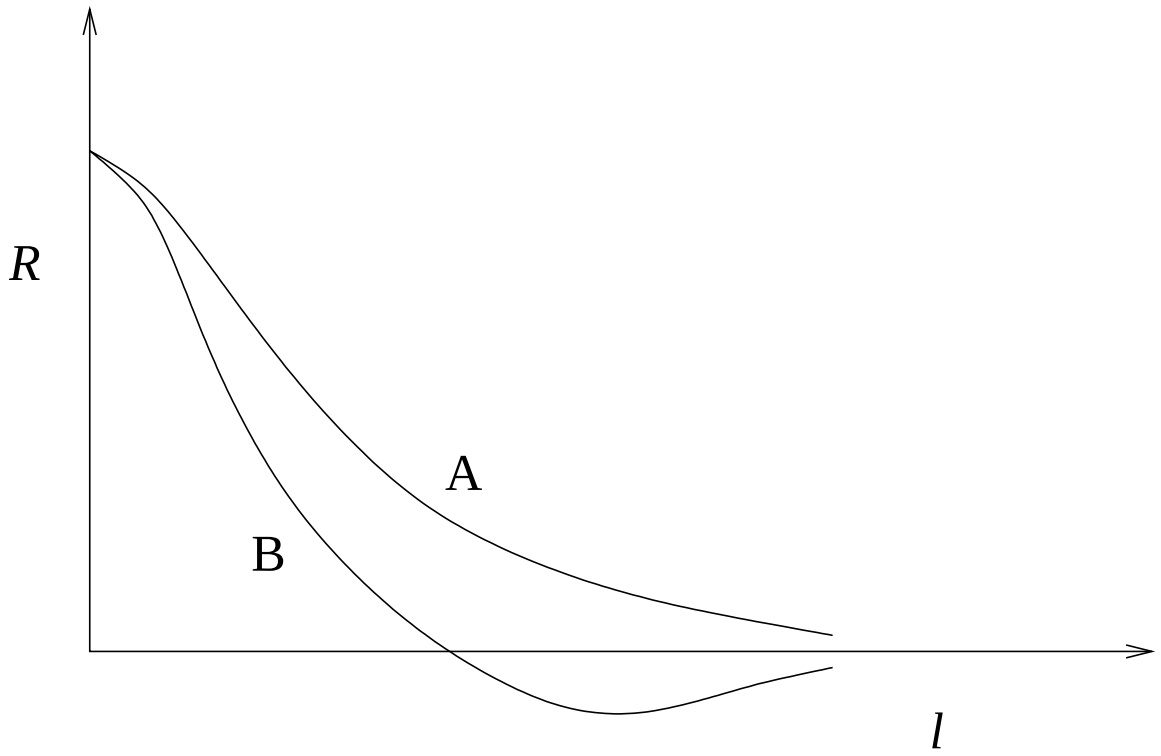

Figure 2: Typical correlation curves. R is the correlation coefficient and l the separation of sample points. For large separation R tends to zero and for no separation $R = 1$.

the experiment which. A rigorous upper bound for the energy spectrum is then presented under the assumption of quasi-geostophy.

3.2 Background on Turbulence (See also [6])

The most successful statistical theory of turbulence is that of Kolmogorov, which involves scaling laws for the structure function $S_p(l) \equiv \langle \delta v(l)^p \rangle \sim l^{\zeta_p}$ of velocity increments $\delta v(l) = v(x+l) - v(x)$, where l denotes the separation between two points. An often studied and very important question regarding turbulence is whether the statistics are self-similar across a wide range of spatial scales, or equivalently whether the probability distribution functions (PDFs) of the velocity increments have a functional form independent of the separation l.

Correlation curves such as in Figure 2 provide a method to study the scale and structure of turbulent motion. Supposing u_1 and u_2 are deviations from the mean flow at different positions but at the same instance, $\overline{u_1 u_2}$ is known as a space correlation. Usually most attention is given to longitudinal or lateral correlations, i.e. to points separated parallel or perpendicular to the velocity components respectively. Correlations depend on both the direction and magnitude of l and different behaviors in different directions may provide information about the structure of turbulence. When $l = 0$, $u_1 = u_2$ (provided they are in the same direction) and the correlation coefficient R is by definition equal to 1, where $R = \overline{u_1 u_2}/(\overline{u}_1^2 \overline{u}_2^2)^{1/2}$. As l increases the velocity fluctuations become more and more

independent of one another and R asymptotes to 0. A negative region in the correlation curve (figure 2 B) implies that u_1 and u_2 are on average in opposite directions.

A correlation curve therefore gives an idea of the distances over which motions at different points significantly affect one another. This statistical analysis gives rise to the structure functions describing the spatial structure of the turbulent motion.

Using Fourier transforms an equation in terms of spectral functions may be obtained alternatively to the correlation functions. In the inertial range these depend only on the wave number k and the energy dissipation ϵ, $E = E(k, \epsilon)$.

$$E(k) = \frac{1}{t} \int_0^t |\hat{u}(k)|^2 dt \tag{6}$$

and dimensional analysis then gives

$$E(k) = A\epsilon^{2/3} k^{-5/3} \tag{7}$$

where A is a numerical constant. This is the famous 'Kolmogorov -5/3 law' which applies for flows of a high Reynold number under two hypothesis: 1) local isotropy and homogeneity, and 2) the existence of a wave number range independent of viscosity and large-scale properties at sufficiently large Reynolds numbers.

3.3 The Experiment

Kolmogorov's theory was developed without considering rotation, for planetary flows however, such as the Earth's atmosphere and ocean, this assumption may not apply since the Rossby number which measures the relative importance of the inertial and Coriolis forces in the Navier-Stokes equation is small,

$$R = \frac{|\mathbf{u} \cdot \nabla \mathbf{u}|}{2|\Omega \times \mathbf{u}|} = \frac{L}{2U\Omega} \ll 1. \tag{8}$$

The experiment carried out by Swinney using a rotating annular tank was the first to determine the statistical properties of turbulence in a low Rossby number flow. The experimental setup was as follows. An annular tank was filled with water and covered by a solid lid; the inner radius of the tank was 10.8 cm and the outer radius 43.2 cm. The depth of the tank increased from 17.1 cm at the inner radius to 20.3 cm at the outer radius to simulate the β-effect of the earths' surface, for more details see [7]. A counter rotating jet was induced in the flow, by continuous pumping of water in to and out of the tank through two concentric rings at the bottom of the tank. A sketch of the setup is shown in Figure 3 and a more detailed description of it may be found in [5].

The purpose of the pumping at the bottom of the cylinder is to create a shear between the Ekman layer and the fluid in the tank and thus induce turbulence. The rapid rotation of the tank (11.0 rad/s) produces essentially 2D flow, except in the thin Ekman boundary layer at the top and bottom surfaces.

Time series measurements of the azimuthal velocity midway between the inner and outer wall of the tank were taken using hot film probes. In order to find a correlation of

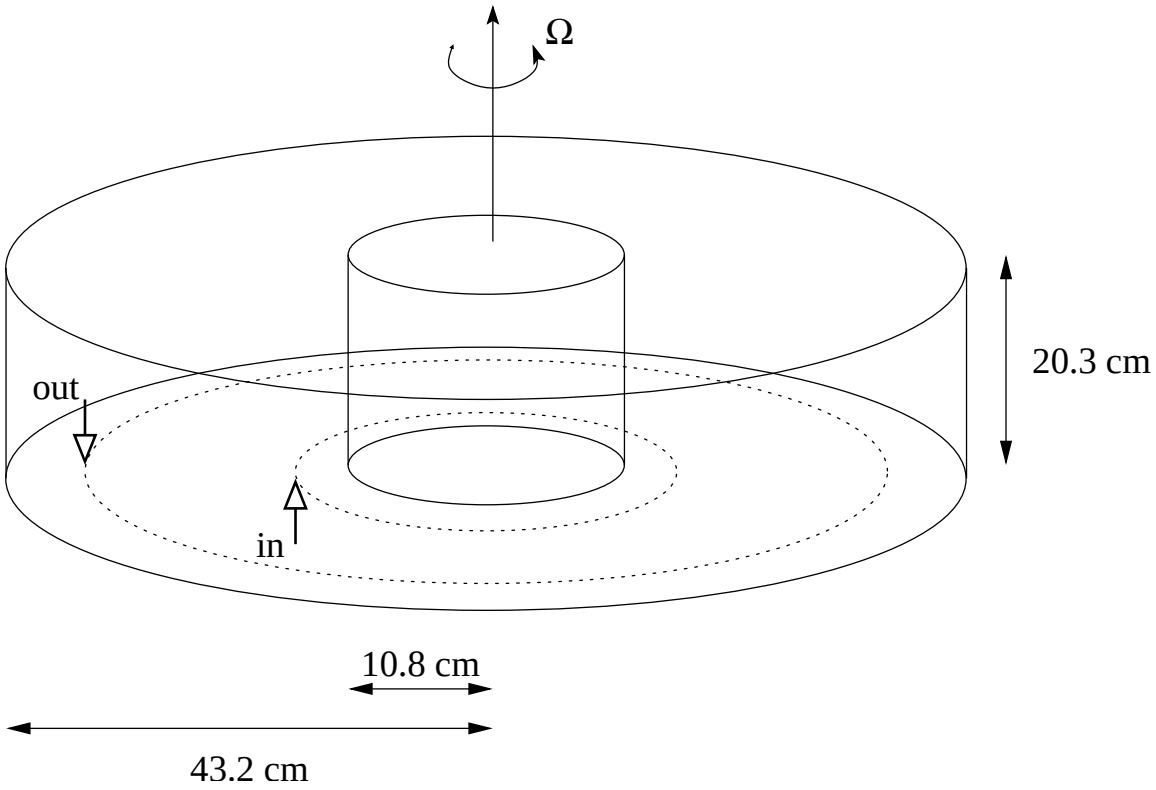

Figure 3: Experimental apparatus. The dimensions of the tank are shown. Note that the tank is covered by a rigid lid. The dotted lines show the approximate positions of the two concentric rings pumping fluid in to and out of the tank, via the inner and outer ring respectively.

the velocity increments an autocorrelation is used, that is, the same velocity components at a single point (the hot film probes) at different instances are correlated. This depends on the time separation s only, however, when the turbulent motion is occurring in a flow with a large mean velocity, as is the case in this experiment ($U_{max} \simeq 22cm/s$), it is possible for the turbulence to be advected past the point of observation more rapidly than the pattern of fluctuations is changing. An autocorrelation will then be directly related to the corresponding space correlation with separation in the mean flow direction, by just transforming the variables, $s = r/U$. This is referred to as Taylor's frozen in turbulence hypothesis.

The energy power spectrum is computed from the time series data obtained in the experiment and they find that $E(k) \sim k^{-2}$ for the inverse energy cascade.

3.4 Inverse Energy Cascade

In two-dimensional turbulence there are two conserved quantities, energy and enstrophy, which are candidates for cascades of the Kolmogorov type (see Figure 4(a)). However, to satisfy both conservation laws there must also be a reverse flow of kinetic energy, from

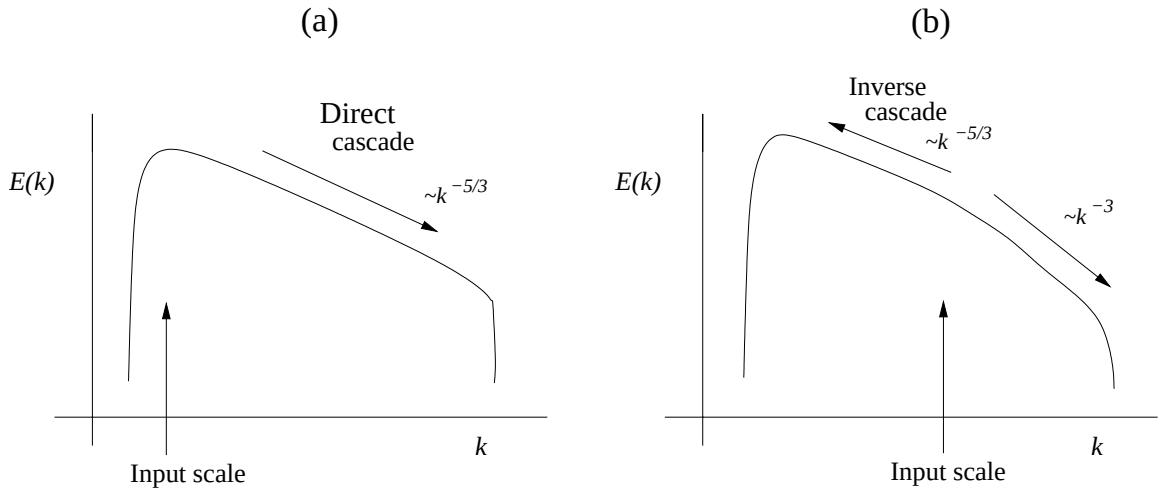

Figure 4: The energy cascade picture of fluid turbulence in (a) 3-dimensions and in (b) 2-dimensions. The input scale is the characteristic wave-number at which the fluid system is forced. In 3-dimensional turbulence energy is transfered inviscidly from the large scales (small k), associated with the energy input scale, to smaller scales where it is dissipated by viscous means at the Kolmogorov lengthscale. In 2-dimensional turbulence kinetic energy can transfer from the input scale up to larger scales. This phenomenon is known as the inverse energy cascade. For a review article on 2D turbulence see [8].

small scales to large scales, called the inverse energy cascade (Figure 4(b)). For strictly two-dimensional Navier-Stokes equations under homogeneous and isotropic conditions the Kolmogorov-Kraichnan theorem predicts a $k^{-5/3}$ inverse energy cascade spectrum at wave-numbers smaller than the forcing scale (for a review of two-dimensional turbulence [8]). In the Experiment which we assume is quasi-2D an inverse cascade is observed as small vortices, an array of vortex filaments are constantly injected at the boundaries of the outlets and inlets, merge to form larger vortices with maximum size limited only by the size of the experimental apparatus.

3.5 Rotating Navier-Stokes Equations

The equations of motion governing a body of fluid rotating at a constant rate about the z-axis are

$$\frac{\partial \mathbf{u}}{\partial t} + \mathbf{u} \cdot \nabla \mathbf{u} + \boldsymbol{\nabla} \pi + 2\Omega \hat{\mathbf{k}} \times \mathbf{u} = \nu \Delta \mathbf{u} \tag{9}$$

$$\boldsymbol{\nabla} \cdot \mathbf{u} = 0$$

$$\pi = \frac{p}{\rho} - \frac{1}{2} \left| \Omega(\hat{\mathbf{k}} \times \mathbf{r}) \right|^2$$

where $\mathbf{u}$ is the relative velocity. The *Coriolis force* $-2\Omega\hat{\mathbf{k}} \times \mathbf{u}$ is always perpendicular to the velocity and hence does no work but tends to deflect moving fluid elements to the right (see [9] for a derivation of these equations). In the Experiment the pumping at the tank bottom produces a counter-rotating jet in the Ekman layer which generates the turbulence observed there.

3.6 Is the Energy Dissipation Bounded in the Experiment?

The Constantin-Doering variational approach can be used to prove the boundedness of the energy dissipation rate for the fluid system studied in the Experiment. The one technical issue is to develop a background field which is continuous, solenoidal and satisfies the necessary boundary conditions.

Natural boundary conditions for the Experiment are no-slip everywhere except at the bottom of the cylinder where fluid is injected through a ring of holes at a rate W and sucked out at the same rate from a concentric ring of holes. The distance between the forcing rings, l, is defined as the integral length scale. We can thus define the boundary conditions as follows

$$\begin{aligned} &\mathbf{u} = W\varphi(\frac{x}{l}, \frac{y}{l})\hat{\mathbf{k}} \quad \text{at } z = 0 \\ &\mathbf{u} = \mathbf{0} \quad \text{otherwise.} \end{aligned}$$

where φ takes the values 1 at the input holes, -1 at the output holes and 0 everywhere else on the bottom boundary.

One can generate a smooth continuation of these boundary conditions in to an incompressible background field U_B as follows: define $\chi(z)$ a smooth function satisfying $\chi(0) = 1$, $\chi'(0) = 0$ and $\chi(H) = 0$, $\chi'(H) = 0$, where H is the height of the cylinder, which decreases rapidly over a small distance δ from $z = 0$ (Figure 5). Now define $\psi(x, y)$ as the two-dimensional solution of

$$\Delta_H \psi + \varphi = 0 \tag{10}$$

where $\Delta_H = \frac{\partial^2}{\partial x^2} + \frac{\partial^2}{\partial y^2}$ is the horizontal Laplacian. Then it is easy to check that the following velocity profile is both incompressible and satisfies the boundary conditions of the experiment

$$U_B(x, y, z) = W \begin{pmatrix} l\chi'(z)(\partial_x\psi)(\frac{x}{l}, \frac{y}{l}) \\ l\chi'(z)(\partial_y\psi)(\frac{x}{l}, \frac{y}{l}) \\ \chi(z)\varphi(\frac{x}{l}, \frac{y}{l}) \end{pmatrix}. \tag{11}$$

Theorem 1: If $\frac{Wl}{\nu} < c$ for some $c > 0$ then $\forall$ initial conditions $\mathbf{u_0}$

$$\limsup_{t\to\infty} \frac{1}{t} \int_0^t \left\langle |\nabla \mathbf{u}|^2 \right\rangle \leq \varepsilon_B \quad \text{where} \quad \varepsilon_B \leq c\,\frac{W^3}{H} \tag{12}$$

Proof idea: This bound on the energy dissipation rate can be calculated using the Constantin-Doering background flow method [10] with background field U_B.

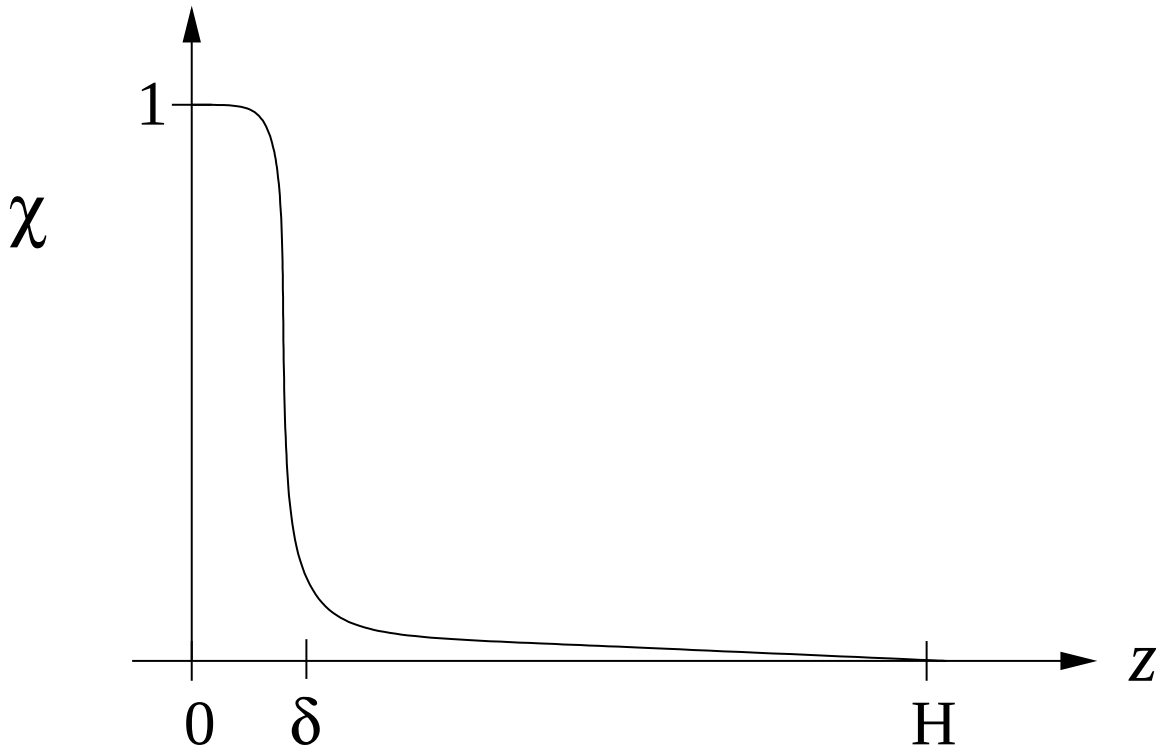

Figure 5: A sketch of the function χ.

A stronger form of Theorem 1 can be proved if we assume that velocity variations in the vertical are much smaller than variations in the horizontal. So assuming that

$$\boxed{\left\langle |\delta w|^2 \right\rangle \leq \gamma \left\langle |\delta u|^2 + |\delta v|^2 \right\rangle}$$

where γ is a small number we can assert a stronger theorem.

Theorem 1a: If $\frac{Wl}{\nu} < c\gamma^{-1/2}$ for some $c > 0$ then $\forall$ initial conditions $\mathbf{u_0}$

$$\limsup_{t\to\infty} \frac{1}{t} \int_0^t \left\langle |\nabla \mathbf{u}|^2 \right\rangle \leq \varepsilon_B \quad \text{where} \quad \varepsilon_B \leq c\,\frac{W^3}{H}$$

3.7 Non-linear Taylor Proudman Theorem

For flows with low values of the Rossby number $Ro = L/(2U\Omega)$, and the Ekman number $E = \nu/(2L^2\Omega)$ a balance between the Coriolis force and the pressure gradient can be assumed in Equation (9), $\boldsymbol{\nabla}\pi + 2\Omega\hat{\mathbf{k}} \times \mathbf{u} = \mathbf{0}$. This balance is called the geostrophic balance. A simple consequence is that $\Omega\hat{\mathbf{k}} \cdot \nabla\mathbf{u} = \mathbf{0}$ or in words $\mathbf{u}$ has no vertical variation

and is therefore two-dimensional. This property of geostrophic flows is known as the Taylor-Proudman Theorem.

A similar theorem has recently been proved for the three-dimensional Euler equations with large Ω. This adds weight to the theoretical study of geostrophic flows for flow scenarios with low Rossby number and $E \ll Ro$. (For example in the Experiment $Ro = O(10^{-2})$ while $E = O(10^{-6})$.)

The momentum equation is now

$$\frac{\partial \mathbf{u}}{\partial t} + \mathbf{u} \cdot \nabla \mathbf{u} + \boldsymbol{\nabla} \pi + 2\Omega \hat{\mathbf{k}} \times \mathbf{u} = \mathbf{0} \tag{13}$$

where $\mathbf{u}$ is again the relative velocity. In the following discussion the vorticity is denoted as $\omega = \boldsymbol{\nabla} \times \mathbf{u}$.

Theorem 2: If we assume that the velocity field $\mathbf{u}$ is smooth and we measure time in units of the local eddy turnover time $|\nabla \mathbf{u}|_\infty^{-1}$, where $|\quad|_\infty$ is the maximum norm, and define $a = \frac{\sup|\omega|}{\Omega}$, then

Two surfaces $z = z_1$ and $z = z_2$ initially separated by a distance $L = z_2 - z_1$ cannot get closer than $(1 - 3a)L$ in each time step.

3.8 Quasi-Geostrophy and $E(k) \sim k^{-2}$

Using the simplest form of the quasi-geostrophic equations [11], which describe the departure from the geostrophic balance for strongly rotating fluids, to produce a rigorous upper bound $E(k) \leq Ck^{-2}$ valid in the inverse cascade region for the energy spectrum can be derived [12]. This *a priori* result supports the inverse energy cascade observed in the Experiment.

Active scalar surface quasi-geostrophic equation

$$\partial_t \theta + \mathbf{v} \cdot \boldsymbol{\nabla} \theta + w_E \Lambda \theta = f \tag{14}$$

with two-dimensional velocity $\mathbf{v}$ incompressible, $\boldsymbol{\nabla} \cdot \mathbf{v} = 0$, and the dissipative term $w_E \Lambda \theta$ has a coefficient $w_E > 0$ that comes from the Ekman pumping at the boundary.

The large forcing scale is defined by

$$k_j^{-1} := \frac{\left\langle k^{-1} |\hat{f}(k,t)|^2 \right\rangle}{\left\langle |\hat{f}(k,t)|^2 \right\rangle} \tag{15}$$

and the theorem states that $E(k) \leq Ck^{-2}$ for $k \leq k_f$ where C is independent of the forcing scale k_f.

References

[1] P. Constantin, C. Hallstrom, and V. Poutkaradze, "Logarithmic bounds for infinite prandtl number rotating convection," Journal of Mathematical Physics **42**, 773 (2001).

[2] C. R. Doering and P. Constantin, "On upper bounds for infinite prandtl number convection with or without rotation," Journal of Mathematical Physics **42**, 784 (2001).

[3] P. Constantin, C. Hallstrom, and V. Poutkaradze, "Heat transport in rotating convection," Physica D **125**, 275 (1999).

[4] P. Constantin and C. R. Doering, "Infinite prandtl number convection," Journal of Statistical Physics **94**, 159 (1999).

[5] C. Baroud, B. Plapp, Z. She, and H. Swinney, "Anomalous Self-Similarity in a Turbulent Rapidly Rotating Fluid," Phys. Rev. Lett. **88**, (2002).

[6] D. J. Tritton, *Physical Fluid Dynamics*, 2nd ed. (Clarenden Press, Oxford, 1988).

[7] J. Pedlosky, *Geophysical Fluid Dynamics*, 2nd ed. (Springer Verlag, New York, 1987).

[8] R. H. Kraichnan and D. Montgomery, "Two-dimensional turbulence," Rep. Prog. Phys. **43**, 547 (1980).

[9] S. Chandrasekhar, *Hydrodynamic and hydromagnetic stability* (Clarendon Press, Oxford, 1961).

[10] P. Constantin and C. Doering, "Variational bounds in dissipative systems," Physica D **82**, 221 (1995).

[11] J. Pedlosky, *Geophysical fluid dynamics*, 2nd ed. (Springer, New York London, 1987).

[12] P. Constantin, "Energy Spectrum of Rotating Fluids," (unpublished, 2002).